Hydro and Solvothermal Synthesis of $Cu_xO/g\text{-}C_3N_4$ Nanoparticles for the Photocatalytic Removal of 2, 4-Dichlorophenol in an Aqueous Solution

A. Al Hinai[1], F. Al Marzouqi[2], S.N. Furqan Ali[1], Y. Kim[3], A. T. Kuvarega[4], B.B. Mamba[4], R. Selvaraj[1]*

[1]*Department of Chemistry, College of Science, Sultan Qaboos University, P.O. Box- 36, P.C. 123, Al- Khoudh, Muscat, Sultanate of Oman*

[2]*Department of Applied Sciences, University of Technology and Applied Sciences, Muscat, Sultanate of Oman*

[3] *Department of Chemical Engineering, Kwangwoon University, Seoul 01897, South Korea*

[4]*Institute for Nanotechnology and Water Sustainability Research, University of South Africa Florida Campus, 1709, Johannesburg, South Africa*

***Email**: rengaraj@squ.edu.om; srengaraj1971@yahoo.com

Received: 11.4.2025, Revised: 13.4.2025, 22.4.2025, Accepted: 27.4.2025

ABSTRACT

A series of $Cu_xO/$ $g\text{-}C_3N_4$ nanocatalysts were synthesized through solvothermal and hydrothermal techniques, utilizing $g\text{-}C_3N_4$ ratios ranging from 10% to 30%. The physicochemical properties of the resulting photocatalysts were analyzed using various techniques, including X-ray diffraction, X-ray photoelectron spectroscopy, transmission electron microscopy, ultraviolet-visible diffuse reflectance spectroscopy, EDXs (energy-dispersive X-ray spectroscopy), and scanning electron microscopy. The photocatalytic performance of the synthesized nanomaterials was assessed by measuring the degradation of 2,4-dichlorophenol (2,4-DCP) in an aqueous medium under visible irradiation. The composite materials successfully degraded 2,4-DCP within 240 minutes. The composite containing 30% Cu_2O with $g\text{-}C_3N_4$ achieved a 50% reduction in the initial concentration, while the 20% CuO with $g\text{-}C_3N_4$ surpassed 90% degradation of the initial concentration. Our findings indicate that the incorporation of CuO and Cu_2O on the surface of $g\text{-}C_3N_4$ nanosheets enhances the photocatalytic oxidation of 2,4-DCP in an aqueous suspension. The experimental data demonstrated that the degradation kinetics of 2, 4-DCP adhered to a pseudo-first-order kinetic model. Notably, the 30% $CuO/$ $g\text{-}C_3N_4$ and 20% $Cu_2O/$ $g\text{-}C_3N_4$ composites exhibited effective

DOI: 10.59143/isas.jisas.3.4.UASP5707

degradation of 2, 4-DCP under the tested conditions. The total carbon content was significantly reduced, as verified by the TOC analyzer, and UV-Vis spectroscopy confirmed a substantial decrease in 2,4-DCP concentration within the 240-minute timeframe.

Keywords

Band gap, Copper oxide, Degradation, Hydrothermal, Nanocomposite, 2, 4-DCPs, Visible light

1. INTRODUCTION

Water is the most important resource of life for humans and all living organisms[1]. Water constitutes around 70% of the Earth's plant; however, merely 0.002% of this water is suitable for human use[2]. The scarcity of clean water has posed a significant challenge for humanity for many years[3]. It is estimated that between 10 to 20 million individuals lose their lives annually due to waterborne diseases and related infections[4]. Additionally, approximately 5,000 to 6,000 children perish each day as a result of water-related issues, including diarrhea[5]. Presently, over 780 million people globally lack access to safe drinking water, leading to serious health complications[6]. Polluted water is unsuitable for drinking and daily needs, as it becomes unpleasant and turbid. Water pollutants encompass chemical, physical, and biological factors that impact the aquatic life and consumers of water [6-8]. Advanced oxidation processes are now considered the preferred process for removing water contaminants organic or inorganic. This is attributed to their ability to transferring organic contaminants into CO_2, H_2O, and inorganic composites. Various nanomaterials such as Nano-TiO_2[8,9], WO_3[10], $SrTiO_3$[11], Fe_2O_3[12], and ZnO[13] have been identified as effective photocatalysts for breaking down organic pollutants in water. A significant obstacle in the application of these photocatalysts is the swift recombination of excited electron-hole pairs, which impedes effective charge transfer reactions between the semiconductor and the adsorbed species. Prior research has indicated that capturing the excited electrons at surface sites can extend the lifespan of charge carriers, thus minimizing the direct recombination of electron-hole pairs. There is a growing interest in enhancing the performance of oxide semiconductor materials due to their distinctive characteristics. Among these oxides, copper oxides (Cu_xO), primarily CuO and Cu_2O, are well-known as p-type semiconductors with distinct physical and chemical characteristics. The bandgap of the bulk Cu_2O and CuO range from 1.8–2.5 eV and 1.2–1.9 eV, respectively[14-16]. These characteristics render them exceptionally appropriate for numerous applications in optoelectronic devices, solar cells, phototransistors, photodiodes, transparent conductive electrodes, catalysis, as well as gas and chemical sensors. Different

morphological variations of Cu_xO have been effectively synthesized, such as nanowires, nanoplatelets, nanoneedles, nanodisks, nanobelts, and nanorods, However, its potential use in environmental remediation is limited. Consequently, only a few studies have been conducted on the photocatalytic capabilities of Cu_xO in breaking down common organic pollutants in water[15,16]. In the present study, Cu_xO (I and II) nanoparticles were produced using straightforward hydro- and solvothermal methods, and their photocatalytic efficiency in the degradation of 2,4-dichlorophenol (2,4-DCP) under light exposure was evaluated. Additionally, challenges remain in the effective application of Cu_xO. A significant issue with Cu_xO is the rapid recombination of photogenerated electrons and holes, which greatly hinders photocatalytic efficiency. Consequently, researchers face the challenge of developing a method for the synthesized photocatalyst to mitigate this issue. One potential solution is the creation of heterojunction materials by combining two semiconductors that possess compatible band energy levels. This approach facilitates the overlap of the conduction band (CB) and valence band (VB) of both materials, offering a viable and effective means to address the previously mentioned limitation. Numerous heterostructures have been studied by coupling Cu_xO with various semiconductors, such as TiO_2, ZnO, TaON, $ZnWO_4$, $BiPO_4$, and Bi_2WO_6[17-21]. Among these, the Cu_xO/g-C_3N_4 composite has garnered significant attention due to a small bandgap value compared to pristine g-C_3N_4 (2.7 eV)[22].

2. MATERIALS AND METHODS

2.1 Materials

Melamine (Sigma-Aldrich-USA), copper (II) nitrate trihydrate (Sigma-Aldrich-USA), ethanol , sodium hydroxide (Sigma-Aldrich-USA), distilled water (H_2O), copper(II) chloride dihydrate (Sigma-Aldrich-USA), D-(+)-glucose (Sigma-Aldrich-USA), 2,4-dichlorophenol (Sigma-Aldrich-USA).

2.2 Preparation of Cu_xO/ g-C_3N_4 composites

As presented in Scheme 1, first, CuO was synthesized using the solvothermal method. $Cu(NO_3)_2.3H_2O$ was used as the Cu source, and ethanol provided oxygen. In a 100-mL conical flask, 0.2415 g of $Cu(NO_3)_2.3H_2O$ was dissolved in 75 mL of EtOH under continuous stirring for 30 min. Following this, the solution was transferred to a Teflon autoclave and then placed in an oven at 160 ℃ for 12 h, with a heating rate of 3 ℃/min. For synthesizing copper(I) oxide, 1 mmol of $CuCl_2.2H_2O$ and 3 mmol of NaOH were mixed and reacted in an excess amount.

Next, 0.1705 g of $CuCl_2.2H_2O$ was dissolved in 75 mL of H_2O under vigorous stirring, and 3 mL of NaOH was added dropwise to this solution. A total of 0.4 g of D-glucose was added to the solution as a reducing agent. This solution was stirred for 30 min to reduce Cu from Cu(II) to Cu(I). After 30 min of stirring, the solution was transferred to a Teflon autoclave and heated at 120 ℃ for 12 h, with a heating rate 3 ℃/min. The total mass of the composite among the materials, calculated using 3 mmol of C_3N_4, was 0.276 g. The synthesis of 10%, 20%, and 30% of Cu_2O/C_3N_4 were from 0.0324 g ,0.0715 g and 0.09871 g of $CuCl_2.2H_2O$, from the percentage should be added, 0.2484 g, 0.216 g, and 0.1932 g for C_3N_4, as 90%, 80% and 70% of g-C_3N_4 should be added for the ratio of composite. The method used to synthesize the composite was the same for all ratios. First, g-C_3N_4 was added in 75 mL of H_2O in a ≥100-mL conical flask, and the solution was sonicated for 30 min. Next, $CuCl_2.2H_2O$ was added to the solution and stirred for 15 min. Following this, 3 mmol of NaOH was added to the solution dropwise, Subsequently, 0.4 g of D-glucose was incorporated into the mixture while maintaining continuous stirring for a duration of 30 minutes. The resulting solution was then transferred to a Teflon autoclave and placed in an oven set to 120 ℃ for 6 hours, with a heating rate of 3 ℃ per minute. After hydrothermal and solvothermal processes, the autoclave was opened and the products were collected in an evaporating dish placed in an oven at 80 ℃ for 24 hours and left for drying.

2.3 Characterization

The characteristics of the prepared samples were examined through various analytical methods. The crystalline structure of the synthesized catalysts was analyzed via X-ray diffraction (XRD) utilizing a MiniFlex 600 bench X-ray diffractometer from Japan. This instrument emitted graphite monochromatized CuKα radiation (λ = 1.540 Å) and was fitted with an NaI (T1) detector. The morphology and microstructure of the composites were assessed using field-emission scanning electron microscopy (FE-SEM; Jeol, JSM 7800F, USA). The elemental composition and ratios (specifically Cu:O and C:N) of the samples were determined with an energy-dispersive X-ray spectrophotometer integrated with the FE-SEM. The ultraviolet diffuse reflectance spectrum (UV-DRS) of the samples was recorded in the wavelength range of 200–1400 nm using a SHIMADZU spectrophotometer (model number: A12595800380), with BaSO4 serving as a blank reference. The bandgap values were derived from the absorption edge using the Tauc plot extrapolation method. Degradation analysis was conducted with a UV–visible (UV–Vis) spectrophotometer (SHIMADZU model number:

A124257) and a total organic carbon (TOC) analyzer (SHIMADZU; model number: H54425901501).

2.4 Photocatalytic degradation experiments

For all samples, the experiments was performed inside an isolated setup using condensed water to maintain a stable temperature. The light creating visible light was used as the light source. A total of 100 mg of catalyst was used and 250 mL of 2,4-DCP solution was used from the prepared of 10 ppm in every experiment. For every experiment, 12 samples were used at different times, with 10 mL for each sample. The first sampling was performed during the first 0 min without the catalyst, and the second sampling was performed after 30 min in a dark room for the adsorption test under continuous stirring. Following this, the visible-light LED white (300 Watts) and air generator were turned on and the samples were obtained at 10, 20, 30, 40, 60, 90, 120, 150, 180, and 240 min. Following this, the sample tubes were covered using a dark cloth to prevent the effects of light that could be absorbed by the material.

3 RESULTS AND DISCUSSION

3.1 XRD analysis

XRD was performed to confirm the crystal phases of the synthesized nanoparticles and investigate the crystalline properties of CuO and Cu_2O, which were synthesized using solvothermal and hydrothermal methods, respectively. The obtained XRD patterns were evaluated by comparing the XRD results with the JCPDS reference cards. Fig. 1(a) shows the diffraction peaks of pure Cu_2O and the Cu_2O composite with 10%, 20%, and 30% g-C_3N_4 obtained via the hydrothermal method. The crystalline unit cell exhibited a cubic phase structure in pure Cu_2O. Fig. 1(b) shows the diffraction peaks of the pure CuO sample, along with the composite with the three ratios of g-C_3N_4 prepared using the solvothermal method. For this CuO sample, the crystalline unit cell was monoclinic. The peaks of the crystalline structure pattern of Cu_2O composite samples were found at 29.5°, 36.3°, 42.3°, 61.3°, 73.5°, and 77.3°, corresponding to (110), (111), (200), (220), (311), and (322) plane space groups, respectively. This is consistent with that reported in the JCPDS card no. 01-077-0199[23-25]. In general, the sharper the peaks, the more crystalline the material. Therefore, the sharp peaks shown by the Cu_2O samples indicated higher crystalline quality. Using Scharrur equation, the grain sizes of synthesized Cu_2O were measured. For pure Cu_2O the grain size was at 35 nm this value found to be reduced to 29.5 nm for the composite.For CuO samples, the peaks for the crystalline structure pattern were found at 25.6°, 27.9°, 29.3°, 31.7°, 35.5°, 38.8°, 46.5°, 84°, 52.7°, and 52.8°, corresponding to (110), (002), (-11), (-112), (020), (202), (-113), and

(022) space plane groups, respectively. This is consistent with that reported in the JCPDS card no. 00-041-0254. The grain sizes of CuO was 38.4 nm and 31.1 nm for the composite. The g-C_3N_4 peak found at 27.2° was broad but not sharp; this was attributed to the duplication of amorphous layers in g-C_3N_4. This result indicates that g-C_3N_4 is not crystalline. The g-C_3N_4 typically exhibits a broad peak in its XRD pattern owing to its amorphous nature[26]. This broad peak is a characteristic feature of amorphous materials, which indicates that the material lacks a long-range order and has a disordered structure. In contrast to crystalline materials, which exhibit sharp and well-defined diffraction peaks, amorphous materials exhibit a broad peak that results from the overlapping of many small peaks owing to the lack of a long-range order. This broad peak in the XRD pattern of g-C_3N_4 is typically centered around 27–28° 2θ, which is a characteristic feature of this material[27]. The 10% composite shown in Fig. 1(a) had one peak (similar to g-C_3N_4) but had a lower intensity. This indicates that some materials present in g-C_3N_4 affected the intensity of the material. For 20% and 30% Cu_2O samples, the peaks increased as the percentage of Cu_2O doped with g-C_3N_4 increased. As shown in Fig. 1(b), the same principle but 10% have more peaks from CuO from lower percentage.

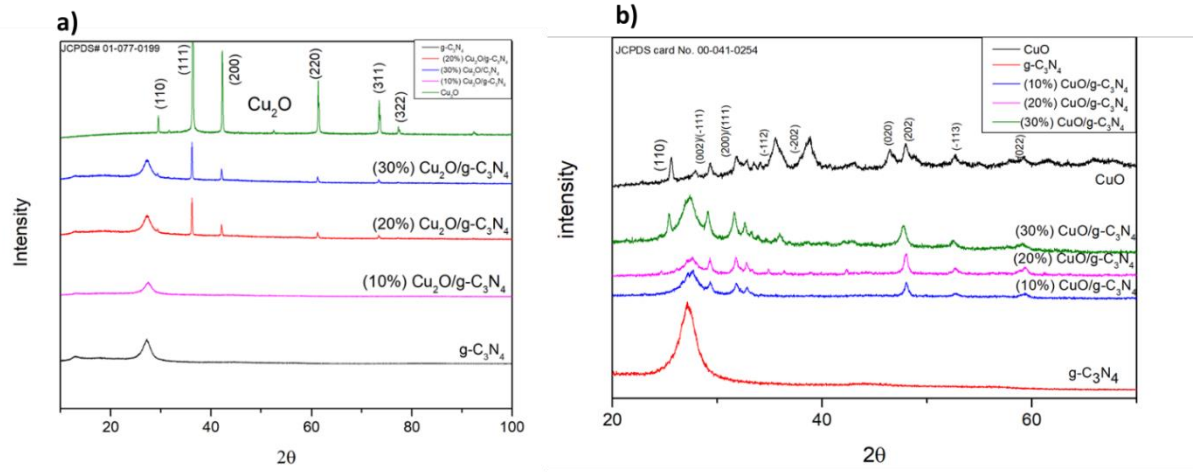

Fig. 1. (a) XRD pattern of Cu_2O nanoparticles (NPs) and composite samples obtained using the hydrothermal method. (b) XRD pattern of CuO NPs and composite samples obtained using the solvothermal method.

3.2 Optical properties

UV–Vis DRS is used to examine the optical and electronic properties by analyzing their absorbance and reflectance in the UV–Vis region of the electromagnetic spectrum. In UV–Vis DRS, a sample is illuminated with light from the UV–Vis region, and the reflected light

is analyzed to determine the electronic transitions that occur in the material. Furthermore, UV–Vis DRS can provide information regarding the bandgap. This technique is particularly useful for studying the electronic structure of materials such as semiconductors and catalysts, which demonstrate electronic transitions in the UV–Vis region[28]. Fig. 2 shows that the materials absorbed light with a wavelength of 400–700 nm from the visible region, except for CuO samples, which absorbed light with a wavelength of approximately 850 nm from the infrared region. The doped material or composite showed a red shift as the percentage of Cu(I) or copper(II) oxide increased (Figs. 2(a) and 2(c)). The g-C_3N_4 sample absorbed light with a wavelength of approximately 470 nm from the visible region, and the Cu_2O sample absorbed light with a wavelength of approximately 600 nm. The Tauc equation is an empirical equation used to determine the optical bandgap of a material from its absorption spectrum. The equation is expressed in the following equation (1):

$$\alpha h\nu = A(h\nu - Eg)^{n/2} \quad (1)$$

where α is the absorption coefficient, $h\nu$ is the photon energy, n is a constant that depends on the nature of the electronic transition (e.g., n=1/2 for directly allowed transitions), A is a constant related to the density of states, and Eg is the optical bandgap.

The bandgap energy is obtained from the slope drawn near the band edge using a Tauc plot. Figs. 2(b) and 2(d) show the bandgaps of synthesized materials. These figures show that, as the percentage of pure Cu(I) or copper(II) oxide increase in the composite, the bandgap approximates that of a pure metal oxide or is reduced. The bandgaps of g-C_3N_4 and 30%, 20%, and 10% Cu_2O were 2.63, 1.65, 1.76, 1.95, and 2.22 eV, respectively, as shown in Fig. 2(d). The bandgaps of CuO and 30%, 20%, and 10% were 1.44, 2.0, 2.22, and 2.5 eV, respectively, as shown in Fig. 2(b). Therefore, the bandgap represents the distance between the VB (the highest occupied energy band) and the CB (the lowest unoccupied energy band) and is used to study the properties of semiconductor materials[30,31].

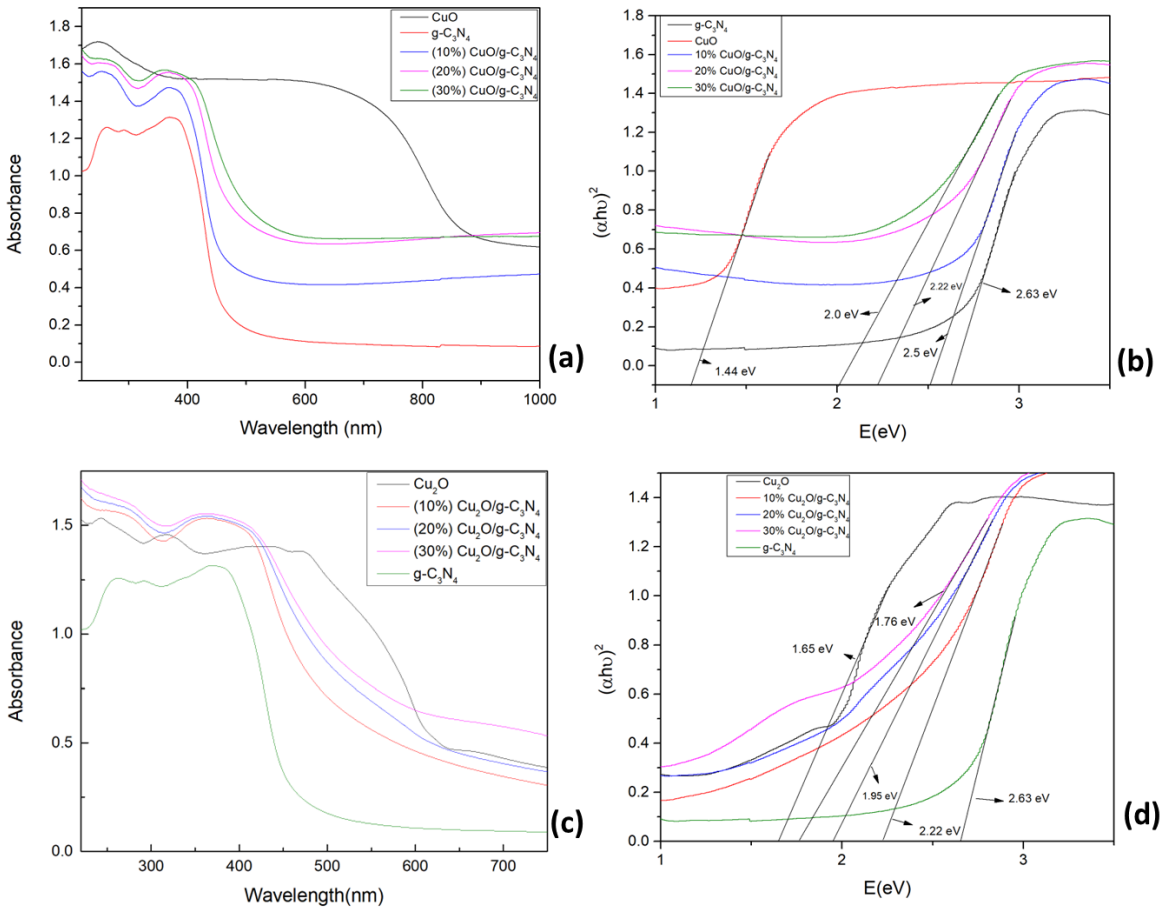

Fig. 2. (a) Absorption wavelength (nm) of CuO and its composites with g-C_3N_4 fabricated using the solvothermal method. (b) Tauc plot showing the bandgap of CuO and its composites with g-C_3N_4. (c) Absorption wavelength (nm) of Cu_2O and its composites with g-C_3N_4. (d) Tauc plot showing the bandgap (eV) of Cu_2O and its composites with g-C_3N_4.

3.3 SEM and EDS Analysis

SEM a type of microscopy that uses a beam of high energy electrons to scan the surface of a sample and generate a highly magnified image of its topography, morphology, and composition. Energy dispersive X-ray spectroscopy (EDS) is used in conjunction with SEM to identify and quantify the elements present in a sample. EDS works by detecting the characteristic X-rays emitted by the sample when it is bombarded with high-energy electrons from an electron beam[32]. The morphology of the synthesized materials was examined via SEM at 1-μm and 100-nm magnification. The results showed that g-C_3N_4 has a two-dimensional nano sheet (Fig. 3), indicating that g-C_3N_4 was synthesized by thermal polymerization. Figs. 4(a)–(d) shows the morphologies of pure CuO and its composites with

g-C_3N_4, which were synthesized using the solvothermal method. Pure CuO demonstrated a spherical zero-dimensional shape. The composite materials it shows have a growth of the CuO material on the surface of the g-C_3N_4 nanosheet and forming like the flower and some places the growth of the material is not complete or not smooth and it formed like sheet but the most morphology of the composite nanoparticle heterojunction between the two material is like flower with high edging which expected to enhance the activity due to the less stability on the sharp edge of the composite nanoparticles. Figs. 3–5 show the morphologies of pure Cu_2O and its composites with 30%, 20%, and 10% g-C_3N_4, which were synthesized using the hydrothermal method. Fig. 5 the shows the morphology of pure Cu_2O, which was cubic or hexagonal. For the composite materials, nanoparticle heterojunctions shown in (b, c, d) indicated an increase in pure Cu_2O on the surface of the g-C_3N_4 nanosheet. Therefore, as the molar ratio of Cu_2O increases, Cu_2O demonstrates a more cubic shape, as shown on the surface of the nanosheet. EDS was also used to identify the components of synthesized samples. A typical EDS spectrum of 30%CuO/g-C_3N_4 is shown in Fig. 6. This confirmed that the synthesized composite materials did not contain any other elemental impurities, and elemental mapping shows the distribution of the metal and elements in nanoparticles, represented by the color of each element in the material (Cu, O, C, and N). Fig. 7 shows the EDS results for the heterojunction 20%Cu_2O/g-C_3N_4, which confirmed that the synthesized material is pure without any elemental impurities. Elemental mapping shows the distribution of elements in the nanoparticles, and each element is represented by different colors, which indicated that the percentage of N and C are higher[32,33].

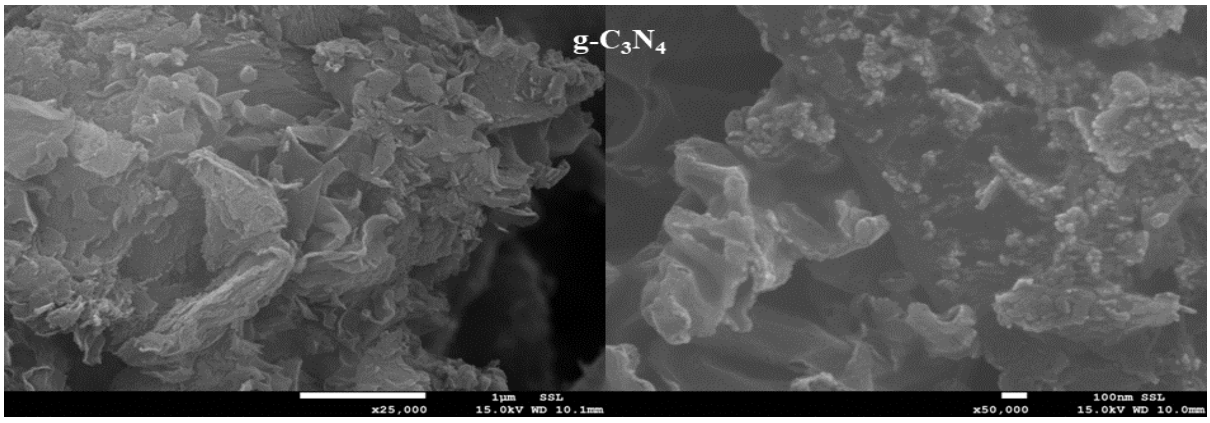

Fig. 3. SEM analysis of g-C_3N_4 synthesized via thermal polymerization.

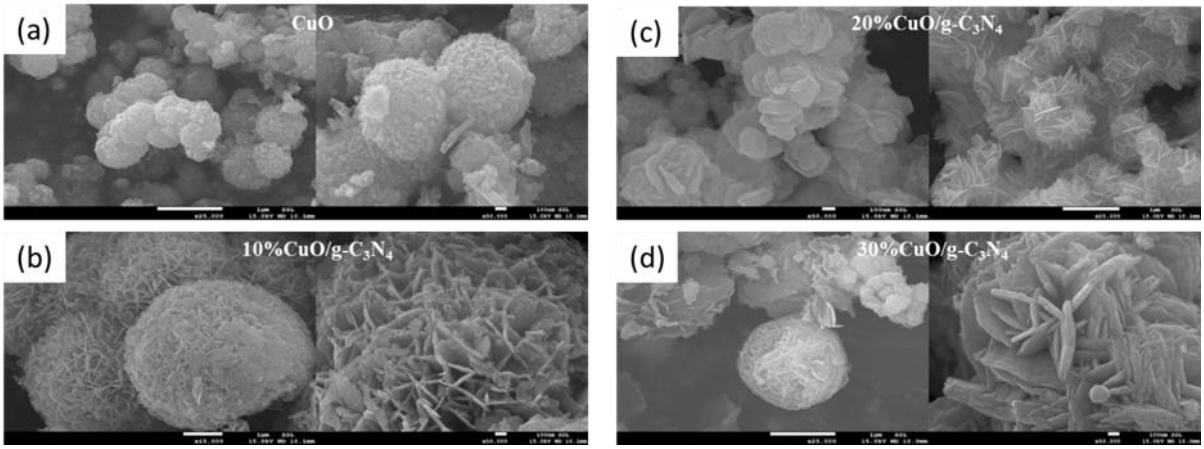

Fig. 4. (a) SEM analysis images of CuO and its composites synthesized using solvothermal method: (b) 10%CuO/g-C_3N_4, (c) 20%CuO/g-C_3N_4, and (d) 30%CuO/g-C_3N_4.

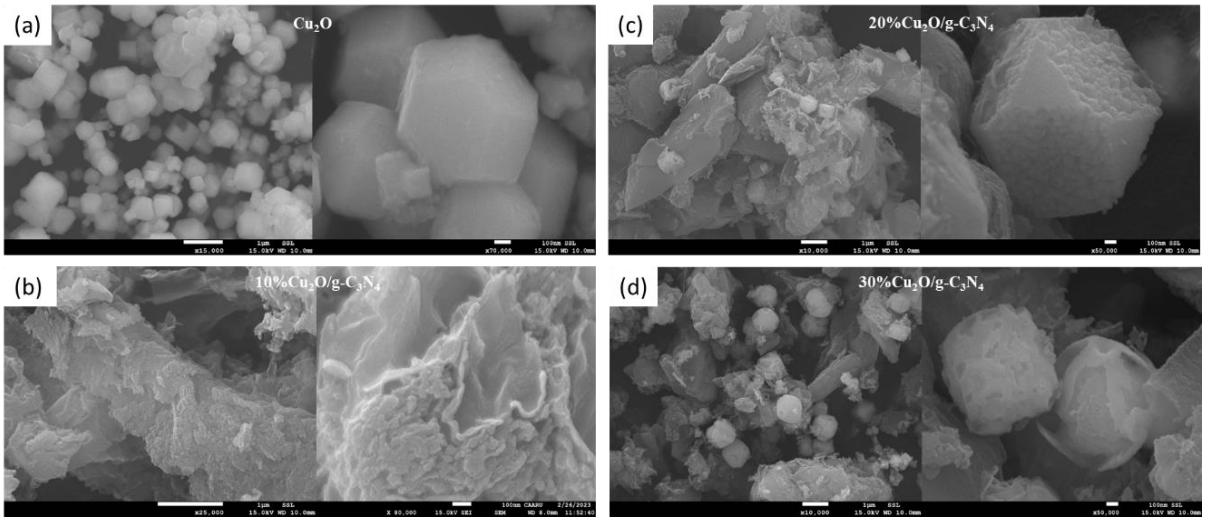

Fig. 5. (a) SEM analysis images of Cu_2O and its composites synthesized using the hydrothermal method: (b) 10%Cu_2O/g-C_3N_4, (c) 20%Cu_2O/g-C_3N_4, and (d) 30%Cu_2O/g-C_3N_4.

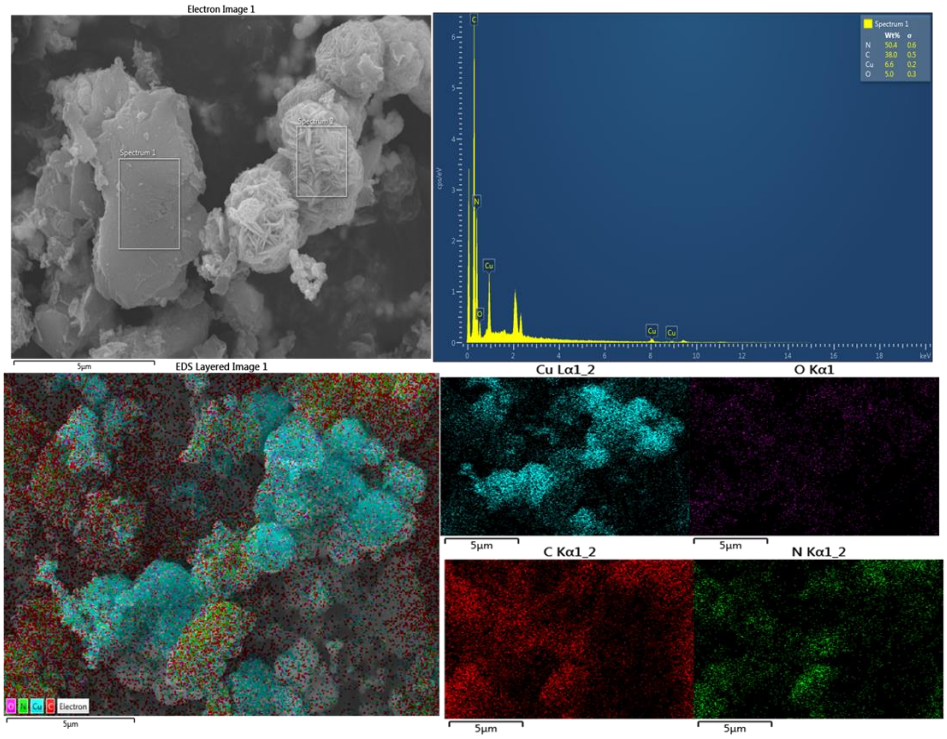

Fig. 6. EDS analysis and elemental mapping images of the composite nanoparticle 30%CuO/g-C_3N_4.

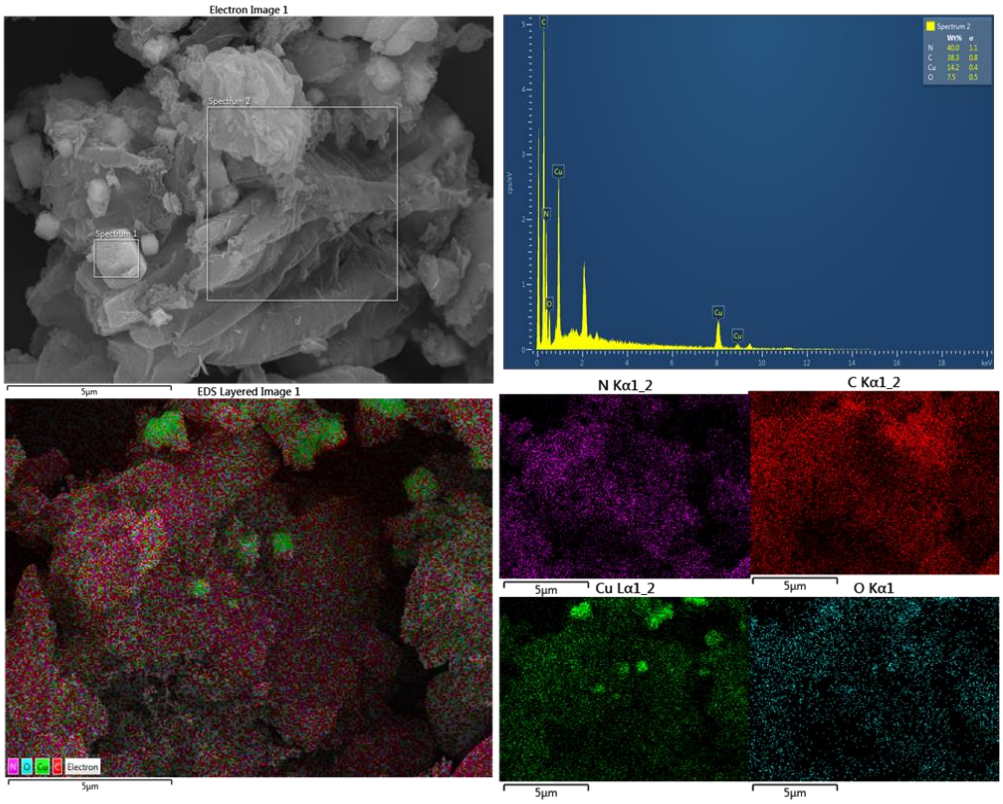

Fig. 7. EDS analysis and elemental mapping images of the composite nanoparticle 20%Cu_2O/g-C_3N_4.

3.4 PHOTOCATALYTIC DEGRADATION OF 2,4-DCP

TOC is a measure of the amount of carbon present in a sample in the form of organic compounds. TOC analysis is commonly used in environmental and water quality testing to determine the amount of organic matter present in a sample, which can be an indicator of pollution or contamination[34-36]. UV–Vis refers to the range of electromagnetic radiation that is visible to the human eye as well as the adjacent UV and near-infrared regions. UV–Vis spectroscopy is a widely used analytical technique that measures the absorption or transmission of light in this range by a sample, providing information about its electronic and molecular structure[37,38]. Fig. 8 shows the best degradation efficiency of the composite material, and with the efficiency of the pure material which doped from using a UV–Vis spectrophotometer and a TOC analyzer. In this study 2,4-DCP was chosen for the degradation study. The λ_{max} of 2,4-DCP is 284 nm which indicates the highest absorbance peak of the pollutant[39]. The degradation efficiency remained the same for all materials over a period of 4.5 h under adsorption (dark). Fig. 8 shows that the synthesized materials are active for the degradation of 2,4-DCP and that the material is successfully doped to obtain a heterojunction material with a better degradation efficiency. Fig. 8(a) shows the degradation results in the UV–Vis region for 20% Cu_2O/g-C_3N_4 under white LED light for 4 h with adsorption (dark). Fig. 8(b) shows that the composite material has better efficiency than the pure material. This indicates that the pollutant concentration is decreased by the time almost is reach < 10% from the original starting concentration, as determined using the TOC analysis. Fig. 8 (c) shows the degradation efficiency of the best heterojunction material (i.e., 30% CuO/g-C_3N_4) collected in the UV–Vis region for 4 h under adsorption (dark). Fig. 8(d) shows a comparison of degradation results between the composite and pure materials, and the results demonstrated that the pollutant concentration was less than 60% of the initial concentration. This result indicate that the synthesized materials are active.

A schematic illustration of the proposed mechanism for the degradation of 2,4-DCP on the surface of Cu_2O/g-C_3N_4 heterojunction under visible light irradiation is shown in Fig. 9. When Cu_2O nano particles are present on the surface of g-C_3N_4, photoexcited electrons from in Cu_2O move from the VB to the CB and are subsequently transferred to the CB of the g-C_3N_4 nanosheet under visible light irradiation (Eqs. (2) and (3)). The electrons could reduce the surface-absorbed oxygen over g-C_3N_4 active sites to form superoxide radicals ($\bullet O_2^-$) (Eq. (4)) and hydrogen peroxide (H_2O_2) (Eqs. (5) and (6)). These reactive species interact with each other to yield hydroxyl radicals (•OH) (Eqs. (7) and (8). However, holes

remained in Cu_2O could react with the surface-absorbed H_2O to generate more $^{\bullet}OH$ (Eqs. (0) and(10))[40].

$$Cu_2O + hv \rightarrow Cu_2O\,(e^-) + Cu_2O\,(h^+) \quad (2)$$

$$Cu_2O\,(e^-) + g\text{-}C_3N_4 \rightarrow Cu_2O + g\text{-}C_3N_4\,(e^-) \quad (3)$$

$$e^- + O_2 \rightarrow O^{\bullet-}{}_2 \quad (4)$$

$$O^{\bullet-}{}_2 + H^+ \rightarrow HO_2^{\cdot} \quad (5)$$

$$HO_2\cdot + HO_2\cdot \rightarrow H_2O_2 + O_2 \quad (6)$$

$$H_2O_2 + e^- \rightarrow \cdot OH + OH^- \quad (7)$$

$$H_2O_2 + O^{\bullet-}{}_2 \rightarrow {}^{\cdot}OH + OH^- + O_2 \quad (8)$$

$$h^+ + H_2O \rightarrow {}^{\cdot}OH + H^+ \quad (9)$$

$$h^+ + OH^- \rightarrow {}^{\cdot}OH \quad (10)$$

$^{\bullet}OH$ leads to the oxidation of 2,4-DCP, leading to the formation of intermediates. These intermediates are subsequently oxidized to finally produce CO_2 and water. In addition, according to previous studies, large amounts of OH groups present on the surface of g-C_3N_4 could also be a reason for high photocatalytic activity[21-23].

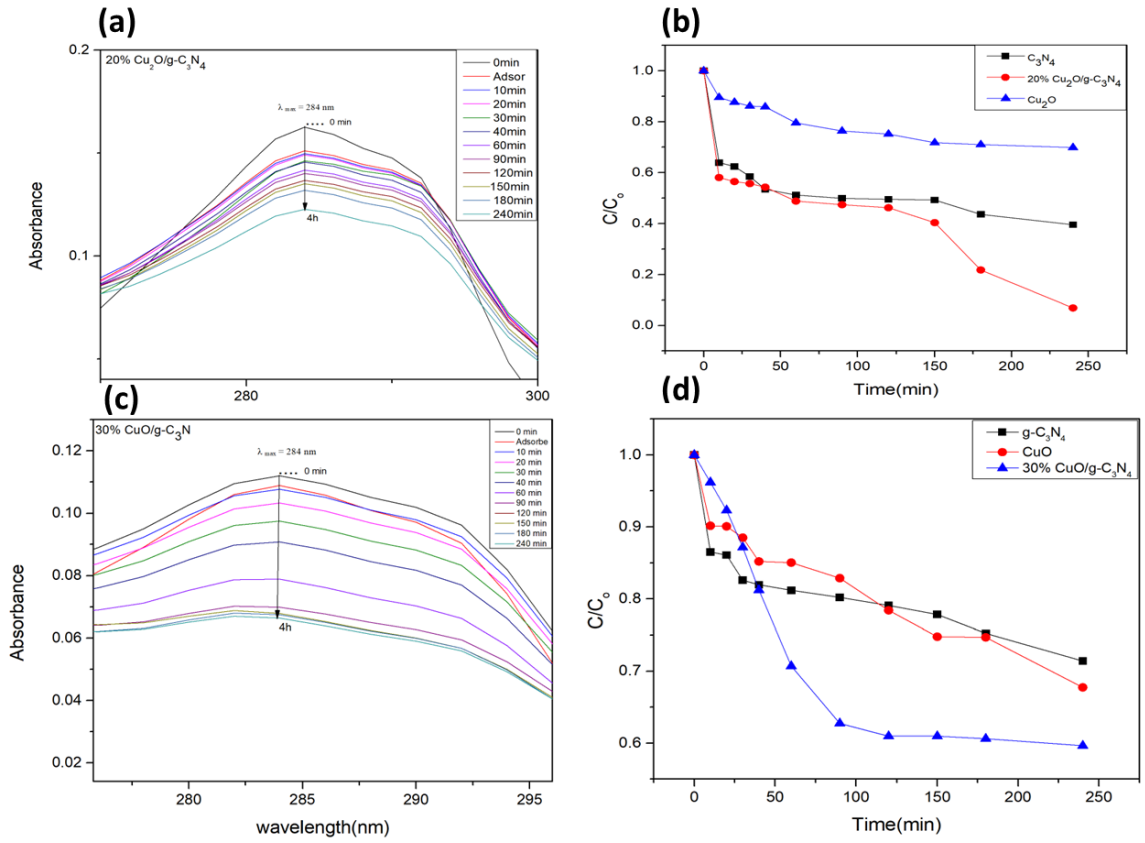

Fig. 8. Photocatalytic degradation of 2,4-DCP by the synthesized materials. (a) Degradation by 20% $Cu_2O/g\text{-}C_3N_4$. (b) C/Co curve of the prepared material obtained using the UV analyzer. (c) Degradation by 30%$CuO/g\text{-}C_3N_4$. (d) TOC result of the composite material.

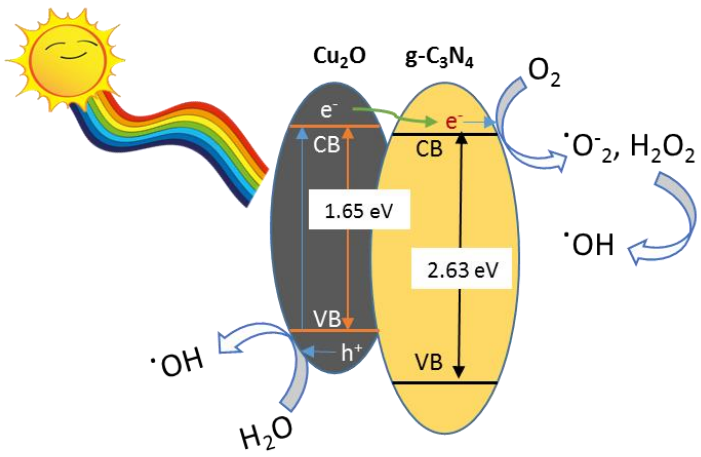

Fig. 9. Schematic illustration of the proposed reaction pathway for the photodegradation of 2,4-DCP by the heterojunction nanomaterial under visible light irradiation.

4 CONCLUSION

In this study, we successfully synthesized pure CuO, Cu_2O, g-C_3N_4, and the composite heterojunction nanoparticles CuO/g-C_3N_4 and Cu_2O/g-C_3N_4 at three different molar ratios of metal oxide (10%, 20%, and 30%) using the solvothermal and hydrothermal methods, respectively, and compared their efficiency in degrading 2,4-DCP present in water under LED visible light in 4 h. The obtained samples (pure CuO, Cu_2O, and the composite with g-C_3N_4 materials) via the hydrothermal and solvothermal methods were characterized using advanced analytical techniques, such as XRD to analyze the crystalline properties, UV–Vis DRS to analyze the optical properties, SEM to analyze the morphology, and EDS to analyze the elemental properties. For photocatalytic application, the efficiency of the prepared materials was evaluated using a UV–Vis spectrophotometer and TOC analyzer. XRD analysis results confirmed the crystalline structure of the synthesized materials. Cu_2O had a cubic crystalline structure and CuO had a monoclinic structure, in accordance with the JCPDS reference. SEM analysis results showed that Cu_2O has a cubic or hexagonal shape, whereas CuO has a spherical shape. EDS analysis was performed to examine whether all synthesized materials were pure, and the results indicated that the materials had no impurities. UV-DRS was used to determine the optical absorption of the material and energy bandgap using the Tauc plot equation. The bandgaps for g-C_3N_4, Cu_2O, and the composite with molar ratios of 30%, 20%, and 10% were 2.63 ,1.65,1.76,1.95, and 2.22 eV, respectively. The corresponding values for CuO were 1.44, 2.0, 2.22, and 2.5 eV, respectively. The UV–Visible spectrophotometer and TOC analyzer were used to determine the pollutant concentration after the degradation of 2,4-DCP over a period of 4 h and for standard calibration. The efficiency of the materials was found to be favorable, and we found that copper(I) oxide with 20% g-C_3N_4 demonstrated the fastest degradation of the pollutant and it reach a molar decrease by lower than 10% and the composite of 30% of copper(II) oxide molar ratio composite material with g-C_3N_4 found to be the most active composite for the degradation of 2,4-DCP under 4 hours and it was reached molar decrease in the concentration lower than 60%. Therefore, the results suggest that the composites of prepared materials increase the efficiency of copper(I) oxide and copper(II) oxide owing to g-C_3N_4 acting as a reducing trapping agent for electrons/holes.

Acknowledgements

Rengaraj Selvaraj acknowledges the Surface Science Lab, Department of Physics, College of Science, Sultan Qaboos University and The Central Analytical and Applied Research Unit

(CAARU) College of Science, Sultan Qaboos University, Muscat, Oman. Also, Prof. Rengaraj Selvaraj greatly acknowledges the University of South Africa for appointed him as Professor Extraodinarius as honorary position.

Author contributions

Abdulrahman Al Hinai: Conceptualization, Methodology, Validation, Investigation, Writing-original draft. Faisal Al Marzouqi: Data Analysis, reviewing - original draft, Formal analysis. Syeda Naheed Furqan Ali - Formal analysis, data curation, investigation. Younghun Kim - reviewing original draft, data analysis, validation. Alex T. Kuvarega – Reviewing original draft, data curation, formal analysis, B. B. Mamba – Reviewing original draft, conceptualization, Rengaraj Selvaraj - Supervision, reviewing - original draft, conceptualization.

Conflict of interest

The authors declare that they have no known competing financial interests or personal relationships that could have appeared to influence the work reported in this paper.

References

1. V. Homem, A. Alves, L. Santos, Amoxicillin removal from aqueous matrices by sorption with almond shell ashes, Int. J. Environ. Anal. Chem., 90, 1063–1084, 2010.
2. R.R. Ismail, N.Z. Kouder, Z.F. Hussein, Verification the Pollution of Tigris River in South of Baghdad using Remote Sensing Techniques., Indian J. Nat. Sci. 9 ,0976–0997, 2018.
3. R. Ahmad, Z. Ahmad, A.U. Khan, N.R. Mastoi, M. Aslam, J. Kim, Photocatalytic systems as an advanced environmental remediation: Recent developments, limitations and new avenues for applications, J. Environ. Chem. Eng. 4, 4143–4164, 2016.
4. B.S. Al Balushi, F. Al Marzouqi, B. Al Wahaibi, A.T. Kuvarega, S.M. Al Kindy, Y. Kim, R. Selvaraj, Hydrothermal synthesis of CdS sub-microspheres for photocatalytic degradation of pharmaceuticals, Appl. Surf. Sci. 457, 559–565, 2018.
5. X. Chen, S. Shen, L. Guo, S.S. Mao, Semiconductor-based photocatalytic hydrogen
6. F. Fresno, R. Portela, S. Suárez, J.M. Coronado, Photocatalytic materials: recent achievements and near future trends. J. Mater. Chem.-Istry A 2. 9,2863-2884, 2014.

7. J. Liu, Y. Zhang, L. Lu, G. Wu, W. Chen, Self-regenerated solar-driven photocatalytic water-splitting by urea derived graphitic carbon nitride with platinum nanoparticles. Chem. Commun. (Camb). 48, 8826–8828, 2012.
8. J. Tauc, R. Grigorovici, A. Vancu, Optical properties and electronic structure of amorphous germanium, physica status solidi (b). 15, 627–637,1966.
9. F.A. Al Marzouqi, N.A. Al-Balushi, A.T. Kuvarega, S. Karthikeyan, R. Selvaraj, Thermal and hydrothermal synthesis of WO3 nanostructure and its optical and photocatalytic properties for the degradation of Cephalexin and Nizatidine in aqueous solution Mater. Sci. Eng. B. 264, 114991, 2021.
10. F.T. Al Sarihi, F.A. Al Marzouqi, A.T. Kuvarega, S. Karthikeyan, R. Selvaraj, Easy conversion of BiOCl plates to flowers like structure to enhance the photocatalytic degradation of endocrine disrupting compounds Mater. Res. Express. 6, 125537,2020.
11. M.A. Meetani, A. Alaidaros, S. Hisaindee, A. Alhamadat, R. Selvaraj, F. Al Marzouqi, M.A. Rauf, DESALINATION AND WATER TREATMENT 138, 270–279, 2019.
12. F. Al Marzouqi, Y. Kim, R. Selvaraj, Shifting of the band edge and investigation of charge carrier pathways in the CdS/g-C3N4 heterostructure for enhanced photocatalytic degradation of levofloxacin, New J. Chem. 43, 9784–9792, 2019.
13. F. Al Marzouqi, R. Selvaraj, Y. Kim, Thermal oxidation etching process of g-c3n4nanosheets from their bulk materials and its photocatalytic activity under solar light irradiation Desalin. Water Treat. 116, 267–276, 2018.
14. F.A. Al Marzouqi, R. Selvaraj, Y. Kim, Mater. Rapid photocatalytic degradation of acetaminophen and levofloxacin using g-C3N4 nanosheets under solar light irradiation Res. Express. 6, 125538, 2020.
15. Ighalo, Joshua O., et al. CuO nanoparticles (CuO NPs) for water treatment: A review of recent advances, Environ. Nano. Mon & Manag 15, 100443, 2021.
16. F. Cheng, H. Yin, Q. Xiang, Low-temperature solid-state preparation of ternary CdS/g-C3N4/CuS nanocomposites for enhanced visible-light photocatalytic H2-production activity, Appl. Surf. Sci. 391, 432–439, 2017
17. Y. He, Y. Wang, L. Zhang, B. Teng, M. Fan, High-efficiency conversion of CO2 to fuel over ZnO/g-C3N4 photocatalyst, Appl. Cat. B. 168–169, 1–8, 2015.

18. K. Li, S. Gao, Q. Wang, H. Xu, Z. Wang, B. Huang, Y. Dai, J. Lu, In-situ-reduced synthesis of Ti3+ self-doped TiO2/g-C3N4 heterojunctions with high photocatalytic performance under LED light irradiation, ACS Appl. Mater. Interfaces. 7, 9023–9030, 2015.
19. F. Al Marzouqi, B. Al Farsi, A.T. Kuvarega, H.A. Al Lawati, S.M. Al Kindy, Y. Kim, R. Selvaraj, Controlled Microwave-Assisted Synthesis of the 2D-BiOCl/2D-g-C3N4 Heterostructure for the Degradation of Amine-Based Pharmaceuticals under Solar Light Illumination, ACS Omega. 4, 4671–4678, 2019.
20. S.-H. Jung, E. Oh, K.-H. Lee, Y. Yang, C.G. Park, W. Park, S.-H. Jeong, Sonochemical preparation of shape-selective ZnO nanostructures, Cryst. Growth, Des. 8, 265–269, 2008.
21. Lei, D. Liu, J. Zhang, P. Zhu, Q. Cui, G. Zou, Direct synthesis, growth mechanism, and optical properties of 3D AlN nanostructures with urchin shapes, Cryst Growth & Des. 9, 1489–1493, 2009.
22. B.G. Streetman, S. Banerjee, Solid State Electronic Devices; Vol. 4, Prentice Hall, New Jersey, 2000.
23. R.F. Pierret, Semiconductor Device Fundamentals, Pearson Education, India, 1996.
24. S.M. Sze, Semiconductor devices, Phys. Technol., John Wiley & Sons 2008.
25. Y. Singh, Semiconductor Devices, IK International Pvt Ltd., 2013.
26. R. Zsigmondy, Colloids and the Ultramicroscope: a Manual of Colloid Chemistry and Ultramicroscopy, J. Wiley & Sons, 1909.
27. Ex, L; INNO, N, International Journal of Engineering and Advanced Technology, Int. J. Eng. Adv. Technol. 2, 1–100, 2013.
28. J. Park, J. Joo, S.G. Kwon, Y. Jang, T. Hyeon, Synthesis of monodisperse spherical nanocrystals. Angew. Chem. Int. Ed. 46, 2007.
29. K. Schafthaul, Gelehrte anzeigen bayer, Akad. 20, 557–561, 1845.
30. K. Byrappa, M. Yoshimura, Handbook of Hydrothermal Technology, William Andrew Publishing, New York, 2001.
31. X. Qu, P.J. Alvarez, Q. Li, Applications of nanotechnology in water and wastewater treatment, Water Res. 47, 3931–3946, 2013.
32. A.D. McNaught, A. Wilkinson, IUPAC Gold Book, Blackwell Scientific Publications, Oxford, 1997.

33. K. Mori, H. Yamashita, M. Anpo, Photocatalytic reduction of CO 2 with H2o on various titanium oxide photocatalysts. RSC Adv. 2, 3165–3172, 2012.
34. K. Pirkanniemi, M. Sillanpää, Heterogeneous water phase catalysis as an environmental application: a review, Chemosphere. 48, 1047–1060, 2002.
35. S. Rosa, A. Nossol, E. Nossol, A.J. Zarbin, P.G. Peralta-Zamora, Non-synergistic UV-A photocatalytic degradation of estrogens by nano-TiO 2 supported on activated carbon, J. Braz. Chem. Soc. 28, 582–588, 2017.
36. A. Mills, R.H. Davies, D. Worsley, Water purification by semiconductor photocatalysis., Chem. Soc. Rev. 22, 417–425, 1993.
37. M. Li, L. Yang, C. Mu, Y. Sun, Y. Gu, D. Chen, T. Liu, H. Cao, Gut, Gut microbial metabolome in inflammatory bowel disease: From association to therapeutic perspectives. Comp. Struct. Biotechnol. J. 20, 2402–2414, 2002.
38. P. Dogra, J.D. Butner, Y.-L. Chuang, S. Caserta, S. Goel, C.J. Brinker, V. Cristini, Z. Wang, , Biomed. Microdevices. 21, 40, 2019.
39. Q. Liu, A. Zhang, R. Wang, Q. Zhang, D. Cui, Mathematical modeling in cancer nanomedicine: a review, Nano Micro Lett. 13, 1–53, 2021.
40. P. Shoghi, M. Hamzehloo, Facile fabrication of novel Z-scheme g-C3N4 nanosheets/Bi7O9I3 photocatalysts with highly rapid photodegradation of RhB under visible light irradiation. J. Colloid Interface Sci. 616, 453–464, 2022.